AIAA 80-1390R

Computational Transonic Inverse Procedure for Wing Design

Vijaya Shankar* and Norman D. Malmuth†
Rockwell International Science Center, Thousand Oaks, Calif.
and
J. D. Cole‡
University of California, Los Angeles, Calif.

A computational transonic inverse procedure for three-dimensional wings in which shapes are determined supporting prescribed pressures is presented. The method is based on modified small disturbance (MSD) theory and can handle wing design in the presence of a fuselage. A consistent analysis-inverse differencing is implemented at the wing slit grid points to ensure recovery of specified pressures in the analysis mode. Formation of an open or a fishtail trailing edge is avoided by a systematic alteration of the velocity potential in front of the leading edge of span stations under inverse mode, until closure is achieved. To lend support to the numerical procedure, an analogous incompressible two-dimensional problem is studied analytically. As an illustration of the usefulness and versatility of the method, the development of a laminar flow control (LFC) wing from a given base wing geometry is presented along with the analysis verification.

Nomenclature

B_n = coefficients used in Eq. (12)
C = net source strength
C_p = pressure coefficient
j,k,ℓ = grid index along x,y,z
M_∞ = freestream Mach number
r = $\sqrt{x^2+y^2}$
u,v = Cartesian velocity component
x,y,z = Cartesian coordinate system
Z = wing surface ordinate
α = freestream angle of attack
γ = specific heat ratio
τ = wing twist
ρ = radius of curvature
ϕ = velocity potential
ξ,σ,θ = dummy variable used in integration

Introduction

CURRENTLY, the aircraft industry is in need of quick turnaround methods to develop energy efficient transonic configurations with optimal aerodynamic characteristics. Development of computational transonic methods over the last decade has contributed significantly toward fulfilling this need by aiding the design of efficient transonic airfoil sections and wing surfaces. Although computational models have been developed primarily to treat the direct problem of determining the load characteristics of a prescribed shape, the inverse problem associated with determining the required recontouring of a given wing to provide a preassigned favorable loading is becoming increasingly important to eliminate much of the cut-and-try approach to geometry definition.

Computational inverse procedures for transonic airfoils have been in use for many years. Early treatments of the problem were given by Nieuwland,[1] who employed hodograph methods to calculate shock-free supercritical flow about a family of quasielliptical airfoils. Later, Garabedian and Korn[2] developed a more general hodograph procedure to design highly cambered shock-free airfoils. In spite of their usefulness, hodograph procedures for design purposes have several disadvantages. They require too many input parameters, are restricted to shock-free solutions, and are not easily extendable to design of three-dimensional wings. Steger and Klineberg[3] treated the problem within a small-disturbance framework solving the continuity and vorticity equation at interior points. To insure consistency between the analysis and the design formulation, they applied appropriate discretization procedures to the vorticity equation at the airfoil grid points. However, the first-order system with velocity components as dependent variables produces a difficulty in the treatment of singularities at the airfoil nose and trailing edge. The effect of nose and trailing-edge singularities could be greatly reduced by using a scalar formulation involving the velocity potential. Tranen[4] employed the full potential equation to remedy the deficiency inherent in the small disturbance formulation at the leading and trailing edges. To overcome the inaccuracies and inconsistencies associated with the discretization procedures at the boundary, iterations had to be employed between direct and inverse solvers in his method. Later, Carlson[5] used dummy point and higher-order accurate methods to handle airfoil boundary points. Rather than employing the circle plane as in Tranen's procedure, Carlson used a Cartesian framework.

Inverse procedures in three dimensions for wing design have been developed only recently by various investigators.[6-12] In Ref. 6, the small disturbance method provides geometric versatility in designing fairly arbitrary geometries. However, the limitation of the method involves the breakdown of the theory for large flow deflections such as those near the leading edge. A full potential inverse method that can treat the leading edge more accurately based on the nonconservative form of the full potential equation was developed by Henne.[7] However, because of the nonconservative implementation, the method of Ref. 7 can lead to erroneous shock solutions. Another method, known as the "fictitious gas" approach,[8-11] is oriented toward achieving shock-free designs, but does not address the problem of determining shapes supporting preassigned pressure distributions handled by the previously cited inverse procedures. There are many applications in which this capability is essential.

Besides the foregoing, another class of procedures is based on optimization methods.[12] Although of considerable

Presented as Paper 80-1390 at the AIAA 13th Fluid and Plasma Dynamics Conference, Snowmass, Colo., July 14-16, 1980; submitted Aug. 12, 1980; revision received Dec. 7, 1981.

*Member Technical Staff. Associate Fellow AIAA.
†Manager, Fluid Dynamics Group. Associate Fellow AIAA.
‡Professor, Structures and Mechanics Department. Fellow AIAA.

usefulness, they require excessive computational effort as compared to the inverse approaches to obtain design solutions.

Toward obtaining a generally useful procedure, this paper will address refinements required to obtain physically meaningful solutions in the inverse method of Ref. 6. In this connection, the issue of "closure" arises in which prescription of arbitrary pressure distributions within inverse formulations such as Ref. 6 can lead to open or fishtail trailing edges. Further development of this method is presented here which removes these defects and achieves closed trailing edges. In the process to be described, closure is obtained by systematic alteration of the velocity potential at various span stations along the wing leading edge.

In general, the method is used in a mixed analysis-inverse mode where at certain span stations geometry will be specified and desired pressures are given on the rest of the wing. As a test of the procedure, an accurate calculation of the flow about the closed airfoil shapes designed by the method verifies the pressure distribution. To lend further support to the method, an analogous incompressible two-dimensional design problem is studied. It should be noted in this respect that the transonic procedure developed here and in Ref. 6 is strictly speaking a *redesign* or perturbation procedure, in the sense that shape alterations are sought of airfoils and wings producing undesirable pressure distributions. Thus, a sort of perturbation problem is being addressed in contrast to the absolute inverse problem studied incompressibly in Refs. 13-16, in which a shape corresponding to a prescribed pressure distribution is sought. The well-posedness of the transonic design problem is in more question than the incompressible case. Issues of existence, uniqueness, and stability have not been addressed here. Even for incompressible flow, only trailing-edge closure (in the sense of zero net source strength) has been addressed adequately. The multiple crossing issue appears largely to have been ignored.

Despite these difficulties, the procedure discussed in this paper appears highly useful for engineering applications. Although it represents, strictly speaking, a redesign rather than an absolute design approach, it can produce shapes having more desirable pressure distributions that represent significant perturbations from configurations with undesirable loadings. This is illustrated in the present paper in which the concept of trailing-edge closure using leading-edge velocity potentials as control variables is treated on a laminar flow control (LFC) wing design problem. The objective is to modify a given base wing consisting of airfoils similar to the NACA four digit series to produce given LFC pressures at midspan. The results of that study are reported in this paper along with the analysis check and off-design performance calculations. The analysis check and analytical study of an incompressible formulation lend credence to the method applied in the absence of a more rigorous mathematical discussion for the transonic regime.

From a practical viewpoint, the method as reported in this paper is very inexpensive to use for wing modification requirements to produce desired pressures. A typical redesign calculation including the trailing-edge closure will require 15-20 min of CPU time on the CDC 7600 machine. This is in contrast to optimization programs that usually require at least several hours of computer time for a similar rigorous design task.

Formulation

The modified small disturbance (MSD) equation in conservation law form used in the mixed analysis-inverse procedure of Ref. 6 is kept the same in this paper

$$\left[(1-M_\infty^2)\phi_x-\left(\frac{\gamma+1}{2}\right)M_\infty^{1.75}\phi_x^2+\left(\frac{\gamma-3}{2}\right)M_\infty^2\phi_y^2\right]_x$$

$$+[\phi_y-(\gamma-1)M_\infty^2\phi_x\phi_y]_y+[\phi_z]_z=0 \qquad (1)$$

Referring to Fig. 1, once the desired pressure coefficient C_p is prescribed at half node points $(j-\frac{1}{2},k)$, the perturbation potential at wing slit points can be obtained in terms of the potential value in front of the nose (leading edge) as

$$(\phi_{j,k})_{\substack{\text{wing}\\\text{plane}}}=(\phi_{\text{nose}})_k-\frac{1}{2}\int_{x_{\text{le}}}^{x}\underbrace{(C_p)_{j-\frac{1}{2},k}}_{\substack{\uparrow\\\text{specified}}}\mathrm{d}x,\quad C_p=-2\phi_x \qquad (2)$$

The potentials $\phi_{j,k}$ at the wing plane from Eq. (2) are used as a Dirichlet boundary condition in solving Eq. (1) under inverse mode. After convergence is established, the new upper and lower wing surface slope information $(\phi_z)_{j,k}$ is obtained by satisfying Eq. (1) at wing plane grid points where pressure is specified.

$$[(\phi_z)_{j,k}]_{\substack{\ell=\text{wing}\\\text{plane}}}=\frac{1}{M_\infty^{0.25}}\left\{\left(\frac{\mathrm{d}Z}{\mathrm{d}x}\right)_{j,k,\ell}-(\alpha+\tau_k)\right\}$$

$$=\frac{\Delta z}{2}\left[B(\Delta\phi)_{j,k,\ell}+(A+C)\Delta\phi_{j,k,\ell+1}+\mathfrak{D}_{j,k,\ell}\right.$$

$$\left.+\frac{2}{(\Delta z)^2}(\phi_{j,k,\ell+1}-\phi_{j,k,\ell})\right] \qquad (3)$$

where A, B, and C are functions of grid spacing, τ_k the twist at the kth span station, α the angle of attack, and $\mathfrak{D}$ is made up of all terms in Eq. (1) except the last term ϕ_{zz}. The upper or lower wing surface ordinate is denoted by Z and the corresponding wing slope $(\mathrm{d}Z/\mathrm{d}x)$ appears in Eq. (3). The term $\mathfrak{D}$ includes second derivatives like ϕ_{yy} and ϕ_{xy} whose finite-differenced forms depend on wing plane potentials at $k-1$, k, and $k+1$ span stations. Equation (2) indicates that these wing surface potential values at $k-1$, k, and $k+1$ stations in turn depend on leading-edge velocity potentials at $k-1$, k, and $k+1$, respectively, as denoted by ϕ_{nose} in Fig. 1. Thus, the modified wing slope information $(\phi_z)_{j,k}$ corresponding to a prescribed pressure $(C_p)_{j-\frac{1}{2},k}$ directly depends on the value for leading-edge potentials which can also be interpreted as constants of integration in Eq. (2). Based on these statements one can write

$$[(\phi_z)_{j,k}]_{\substack{\ell=\text{wing}\\\text{plane}}}=\phi_z[\ldots,(\phi_{\text{nose}})_{k-1},(\phi_{\text{nose}})_k,(\phi_{\text{nose}})_{k+1},\ldots] \qquad (4)$$

Now define a trailing-edge thickness parameter t_k for the kth span station such that

$$t_k=\int_{X_{\text{le}}}^{X_{\text{te}}}[\phi_z]_{\substack{\text{wing}\\\text{plane}}}\mathrm{d}x \qquad (5)$$

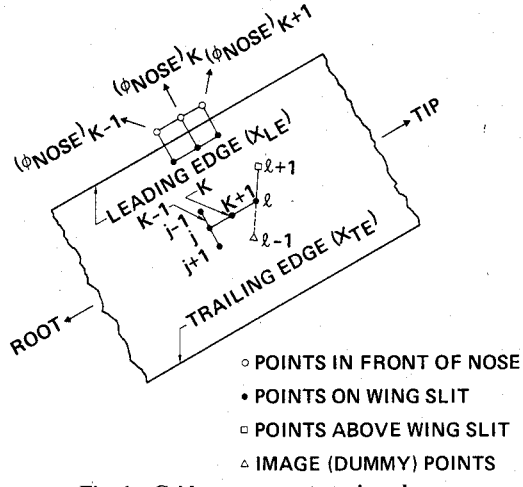

Fig. 1 Grid arrangement at wing plane.

where [ ] denotes $(\phi_z)_{\text{upper surface}} - (\phi_z)_{\text{lower surface}}$, and X_{le} and X_{te} represent leading- and trailing-edge x values, respectively. The thickness parameter t_k is then directly controlled by leading-edge (nose) potential values through ϕ_z whose functional dependence is given in Eq. (4). If t_k is zero, then the kth span station has a closed trailing-edge airfoil, and positive or negative t_k would indicate an open or a fishtail trailing edge, respectively. The objective is to achieve $t_k = 0$ for trailing-edge closure or some prescribed thickness t_k by a suitable alteration of ϕ_{nose} values. Several iterative schemes can be employed for the ϕ_{nose} search process, but the one utilized in this paper is based on a simple Taylor series expansion procedure. Expanding t_k in terms of ϕ_{nose} potentials

$$t_k[(\phi_{\text{nose}} + \Delta\phi_{\text{nose}})] = t_k(\phi_{\text{nose}}) + \left[\frac{\partial t_k}{\partial(\phi_{\text{nose}})_m}\right]\Delta(\phi_{\text{nose}})_m + \cdots$$

$$m = k_s, \ldots, k-1, k, k+1, \ldots, k_e$$

$$k = k_s, \ldots, k-1, k, k+1, \ldots, k_e \tag{6}$$

where k_s and k_e denote the first inboard and final outboard span stations under design mode, respectively. For trailing-edge closure condition, the left-hand side of Eq. (6) is set to zero which yields enough equations to uniquely solve for all $(\Delta\phi_{\text{nose}})_m$

$$\{\Delta\phi_{\text{nose}}\} = -\left[\frac{\partial t_k}{\partial(\phi_{\text{nose}})_m}\right]^{-1}\{t_k\} \tag{7}$$

The $\{\Delta\phi_{\text{nose}}\}$ solution vector from Eq. (7) gives the amount of alteration to be made on $\{\phi_{\text{nose}}\}$ to drive $\{t_k\}$ to zero. In Eq. (7), the { } symbol denotes a vector and $[\ ]^{-1}$ denotes the inverse of a matrix. Each element of this matrix is a partial derivative and a complete evaluation of all the matrix elements and the subsequent matrix inverse can be very costly and time consuming, especially if several span stations are under design mode. To reduce substantially the computer time in the evaluation of matrix elements in Eq. (7), some tricks are used. First, the span station which has the maximum positive or negative thickness is selected. For this span station (call it $k = k_t$) the influence function $\partial t_k / \partial(\phi_{\text{nose}})_{k_t}$ is generated and that influence function distribution is kept the same for all other design span stations but the magnitude is scaled by the following:

$$\frac{\partial t_k}{\partial(\phi_{\text{nose}})_m} = \left(\frac{\partial t_k}{\partial(\phi_{\text{nose}})_{k_t}}\right)\frac{\dfrac{\Delta t_m}{\Delta(\phi_{\text{nose}})_m}}{\dfrac{\Delta t_{k_t}}{\Delta(\phi_{\text{nose}})_{k_t}}} \tag{8}$$

$$m = k_s, \ldots, k-1, k, k+1, \ldots, k_e$$

Use of Eq. (8) has drastically reduced the time taken to evaluate the solution vector $\{\Delta\phi_{\text{nose}}\}$ from Eq. (7). Also, in the evaluation of the matrix inverse appearing in Eq. (7), the elements of the matrix other than the tridiagonal terms are thrown away.

The following steps summarize the inverse solution procedure.

1) Compute the analysis flowfield for the given initial base wing geometry.

2) Compute the wing plane velocity potential from Eq. (2) corresponding to the desired modified pressure distribution. Use ϕ_{nose} initially from the analysis calculation of step 1.

3) Compute the solution corresponding to the Dirichlet boundary condition from step 2 and the new wing slope information from Eq. (3). Then compute t_k from Eq. (5).

4) To achieve trailing-edge closure, modify ϕ_{nose} according to Eq. (7).

5) Repeat steps 3 and 4 until trailing-edge closure is achieved.

Analysis of Incompressible Prototype of Closure Procedure

The quantitative results to be presented are obtained from a computational inverse method which modifies a pressure distribution associated with a known airfoil or wing shape. The central idea utilized to obtain trailing-edge closure is based on the assertion that open or fishtailed shapes which arise in the process of solving the Dirichlet problem for the perturbation potential ϕ can be driven to closed contours by systematically and iteratively adjusting ϕ at some location on the airfoil surface. These ϕ adjustments leave the target pressures invariant.

The method has been tested by verifying, by direct calculation, that the design pressures actually are recovered (see numerical examples of the following section). Some theoretical proof of the method would place it on a firmer foundation. In this connection, previous investigations, such as Ref. 5, have utilized the concept of adjustment of nose radius to achieve closure for two-dimensional flows. Accordingly, the mathematical framework that analyzes the idea should also indicate the connection between the role of the nose potential value ϕ_N, the nose radius of curvature, and the net source strength.

In this section, the closure problem is discussed within the framework of incompressible thin airfoil theory. The conclusions of the incompressible theory support the numerical procedure utilized in transonic flow. The analytical results can be derived from a consideration of the thickness design problem of thin airfoil theory which represents the symmetric part of the full problem. To fix the ideas, consider the symmetric profile shown in Fig. 2.

From well-known formulas of thin airfoil theory, the harmonic boundary value problem for ϕ which seeks a shape given by $\phi_y(x,0+) = v_0(x) = F'(x)$, $-1 \le x \le 1$, corresponding to a prescribed pressure $u_0(x)$, leads to

$$\phi_x(x,0+) \equiv u_0(x) = \frac{1}{\pi}\int_{-1}^{1}\frac{v_0(\xi)\,d\xi}{x-\xi}, \qquad |x| < 1 \tag{9}$$

Reference 17 gives the following general solution of the singular integral Eq. (9):

$$v_0 = -\frac{1}{\pi}\frac{1}{\sqrt{1-x^2}}\int_{-1}^{1}\frac{u_0(\xi)}{x-\xi}\sqrt{1-\xi^2}\,d\xi + \frac{C}{\sqrt{1-x^2}} \tag{10}$$

In Eq. (10) the constant C, analogous to the circulation in the direct problem, is the net source strength. Thus,

$$C = \int_{-1}^{1} v_0\,dx = \text{net source strength} = \frac{F(1)}{\pi}$$

with $F(1)$ the trailing edge thickness. The far field asymptotic behavior of ϕ is

$$\phi = C\log r + \mathcal{O}(r^{-1}) \quad \text{as} \quad r = \sqrt{x^2+y^2} \to \infty$$

We note that, to within a sign of u and v, Eqs. (9) and (10) apply with u and v interchanged to give the solution of the

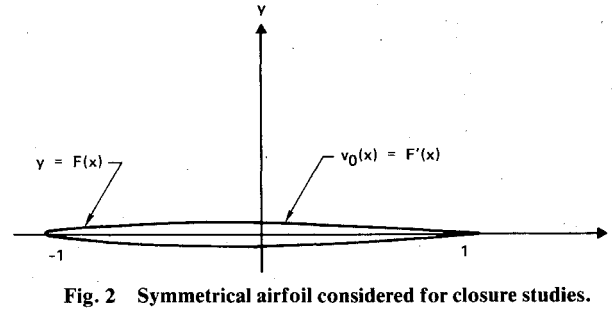

Fig. 2 Symmetrical airfoil considered for closure studies.

antisymmetrical camber problem (v specified and u to be determined).

From Eq. (10) and the equation

$$\phi=\frac{1}{\pi}\int_{-1}^{1} v_0(\xi)\log\sqrt{(x-\xi)^2+y^2}\,d\xi$$

it can be demonstrated that

$$\phi_N\equiv\phi(-1,0)=-C\ell n2-\frac{1}{\pi}\int_{-1}^{1} u_0(\sigma)\cos^{-1}\sigma\,d\sigma \tag{11}$$

The role of leading- and trailing-edge curvature can be illuminated by representing the target pressure distribution as a Fourier series, as in Ref. 18. Thus, if $x=\cos\theta$ and

$$u_0=\frac{\lambda+\tau}{2}+\sum_{n=1}^{\infty}B_n\cos n\theta,\quad B_n=\frac{2}{\pi}\int_0^{\pi}u_0(\theta)\cos n\theta\,d\theta,\quad n\geq 1 \tag{12}$$

$\tau^2/2=\rho_{le}$, the radius of curvature of the leading edge; and $\lambda^2/2=\rho_{te}$, the radius of curvature at the trailing edge; then we obtain from Eq. (10)

$$v_0=-\frac{\lambda}{2}\tan\frac{\theta}{2}+\frac{\tau}{2}\cot\frac{\theta}{2}+\sum_{n=1}^{\infty}B_n\sin n\theta \tag{13}$$

From Eq. (10), it is evident that $C=(B_1+\tau-\lambda)/2$. Thus, the closure condition is

$$C=0=B_1+\tau-\lambda \tag{14}$$

where

$$B_1=\frac{2}{\pi}\int_0^{\pi}u_0(\theta)\cos\theta\,d\theta$$

Equation (13) leads to the important conclusion that closure can be achieved by adjusting one of the following quantities: 1) ρ_{le}, 2) ρ_{te}, and 3) ϕ_N. In fact, in contrast to the numerical iterative procedure for transonic flow, the precise quantitative value of ϕ_N in the linear regime can be determined explicitly once and for all from Eq. (11) for arbitrary pressure distributions given by Eq. (12) as

$$\phi_N=-C\log 2+\frac{\tau+\lambda}{2}+\frac{B_1}{4}+\sum_{n=2}^{\infty}\frac{(-)^nB_n}{n^2-1} \tag{15}$$

which according to Eq. (14) for a closed airfoil becomes

$$\phi_N=\frac{\tau+3\lambda}{4}+\sum_{n=2}^{\infty}\frac{(-)^nB_n}{n^2-1}=-\frac{1}{\pi}\int_{-1}^{1}u_0(\sigma)\cos^{-1}\sigma\,d\sigma \tag{16}$$

This result easily can be generalized to Prandtl-Glauert flows. The extension of these theoretical results to three-dimensional wings currently is being investigated.

The general solution should also have the property of positive volume at any x_0, $|x_0|<1$. If $x_0=\cos\theta_0$, then the positive volume constraint imposes a condition on the B_n given by

$$\int_{-1}^{x_0}v_0\,dx=\frac{B_2}{2}\sin 2\theta_0-(\lambda+\tau)\sin\frac{\theta_0}{2}$$

$$-\frac{1}{2}\sum_{n=2}^{\infty}B_n\left[\frac{\sin(n-1)\theta_0}{n-1}-\frac{\sin(n+1)\theta_0}{n+1}\right]>0 \tag{17}$$

Summarizing, the previous analytical developments demonstrate the soundness of the method utilized in this paper when applied to the incompressible case. No substantive changes in this assessment are anticipated in the transonic regime. Specifically, we have shown the following.

1) For finite leading- and trailing-edge curvature incompressible airfoils, global closure, in the sense that the net source strength on the airfoil given by

$$C=\frac{1}{\pi}\int_{-1}^{1}v_0\,dx$$

will be zero, is achieved providing the nose value of $\phi=\phi_N$ takes on the value given by Eq. (16) without affecting the *prescribed pressures, which are left completely unconstrained.* Moreover, there is a unique combination of leading- and trailing-edge radii associated with this ϕ_N according to Eqs. (12) and (14).

2) The value of ϕ_N is related to the leading- and trailing-edge curvatures through Eq. (16).

3) If both leading and trailing edges have zero radius of curvature, then Eq. (14) gives the integral constraint $B_1=0$ on the class of admissible pressures leading to a closed contour.

4) If the trailing edge is a cusp, i.e., $v_0(1)=0$, an integral constraint on the pressure is required for closure. With $C=0$, this is obtained from Eq. (10) as

$$\int_{-1}^{1}u_0(\xi)\sqrt{\frac{1+\xi}{1-\xi}}\,d\xi=0$$

5) If the trailing edge has a finite angle, the resulting logarithmic singularity of the sharp edge can be achieved by asserting that $B_n=\mathcal{O}(n^{-1})$ as $n\to\infty$ and omitting the second term in Eq. (13). This term will be included for a round edge if, for example,

$$v_0\doteq\frac{a_1}{\sqrt{x-1}}+a_2+\ldots,\quad \text{as } x\to 1,\quad a_2\neq 0$$

If trailing-edge sharpness is rigorously enforced, then Eq. (14) imposes an integral constraint on the pressure distribution. Therefore, an imperceptibly and unimportantly small trailing-edge roundness is introduced by the iterative ϕ_N adjustments with fixed pressure distributions. From Eq. (12) and the asymptotic formulas of Ref. 17, the associated trailing-edge pressure is finite.

6) In transonic flow, the value of ϕ_N must be found iteratively as in the scheme outlined in the preceding section. Here, however, as in the incompressible case, the far field for the intermediate boundary-value problems for ϕ associated with openness has the logarithmic behavior $\phi=C\log r+\mathcal{O}(1/r)$ as $r\to\infty$. This must be updated in the iterative process.

7) The condition

$$\int_{-1}^{x}v_0\,dx=\text{local volume}>0,\quad |x|<1$$

(i.e., no contour crossings or multiple fishtailing) can be enforced by multiple constraints on the prescribed pressure distributions and is given explicitly for incompressible flow by Eq. (17).

Other than those delineated in items 1-7, no further constraints are required in incompressible small disturbance theory. This is in contrast to the requirements imposed by Lighthill[14] for exact potential theory.

Results

The newly developed inverse code with the trailing-edge closure model was put to test to achieve the following objective. Provide the definition of the aerodynamic shape required in the test strip of the wing shown in Fig. 3 to produce the streamwise pressure distribution given in Ref. 19, and reproduced in Fig. 4 at the midspan, at a freestream Mach

number of $M_\infty = 0.84$ and angle of attack $\alpha = 3$ deg. The airfoil geometry at the root section for the basic wing is shown in Fig. 5. The other geometry information provided is the semispan is 318 in., the root chord is 180 in., the tip chord is 56 in., and 1/4 chord sweep is 30 deg. Ordinates at span station η equal root ordinate $\times (1 - 0.25\eta)$ (except in test strip). The twist distribution at span stations 0, 60, and 100% had local twist angle $\tau = 0$, -0.5, and -4 deg, respectively with linear twist variation between stations.

The wing modification results reported here were performed on a CDC 7600 computer using a fine grid consisting of $60 \times 30 \times 20$ points. The inverse calculation is started from the base wing analysis calculation. Initially, in the test strip region (40-60% span), the shapes of the airfoils are chosen to be the same as the rest of the wing. At $M_\infty = 0.84$ and $\alpha = 3$ deg with the initial twist distribution, the base wing produced a pressure distribution on the upper and lower surface as shown in Fig. 6. A shock is present on the upper surface. The pressure distribution produced by the base wing in the test strip region and in particular at midspan is far from the desired midspan pressure distribution as shown in Fig. 4. Accordingly, the objective here is to modify the wing in the test strip region to produce the pressures of Fig. 4 at 50% span.

After the analysis results were established, the code was switched from the analysis mode to inverse mode in the test strip region with pressures in this region modified to those shown in Fig. 7. Here, at midspan the specified pressure is the same as in Fig. 4. With analysis pressures kept fixed at 40 and 60% span, the rest of the specified pressures in the test strip region were linearly interpolated from 40 to 50% and from 50 to 60%. The wing outside of the test strip (0 to 40% and 60 to 100%) was treated as analysis with shape given as before. The inverse calculations were initiated with leading-edge potential ϕ_{nose} values in the test strip region from the analysis run. These analysis ϕ_{nose} values were then systematically altered according to Eqs. (7) and (8) until all the modified airfoils in the test strip region had closed trailing edges within some specified tolerance (usually less than 0.1% of chord). The results from the inverse calculation are shown in Fig. 8. The starting base wing airfoils in the test strip region are shown in Fig. 8a. They are conventional, similar to NACA four digit airfoils. The modified wing with ϕ_{nose} values chosen from the analysis run did not have closed trailing-edge airfoils for all span stations. Some had a fishtail and some had openness, as shown in Fig. 8b. After proper alteration of the ϕ_{nose} values, the final modified wing had trailing-edge closure within a specified tolerance. This is shown in Fig. 8c.

Figures 9, 10, and 11 show similar results at 40, 50, and 60% span, respectively, as in Fig. 8, but clearly illustrate the shape differences between the base wing airfoil, modified airfoil before trailing-edge closure, and final airfoil after trailing-edge closure. The midspan airfoil seems to undergo the most drastic shape alteration as seen in Fig. 10. Along

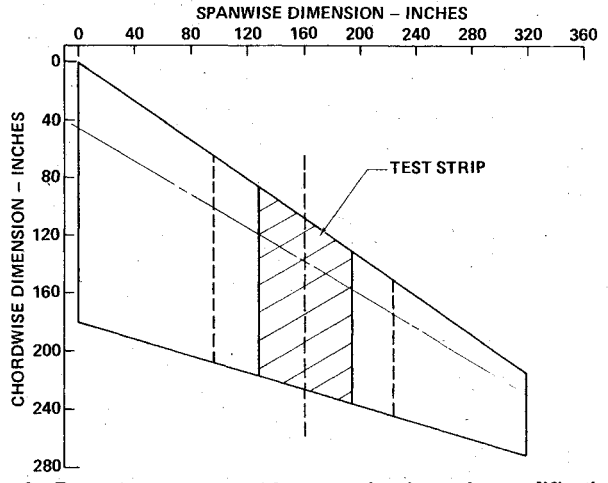

Fig. 3 Base wing geometry with a test strip where wing modification is required.

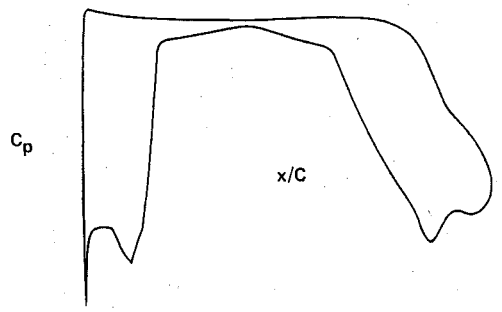

Fig. 4 Desired streamwise pressure distribution.

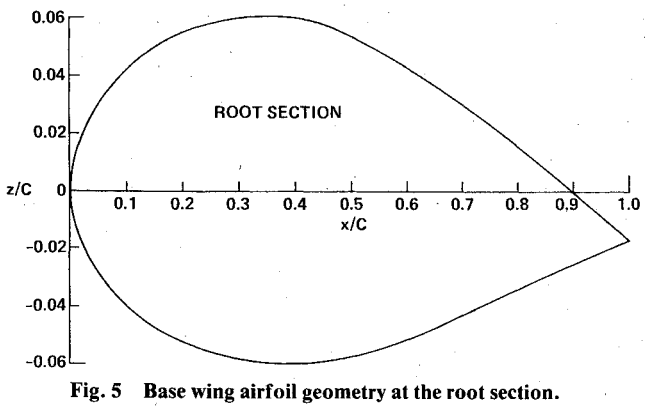

Fig. 5 Base wing airfoil geometry at the root section.

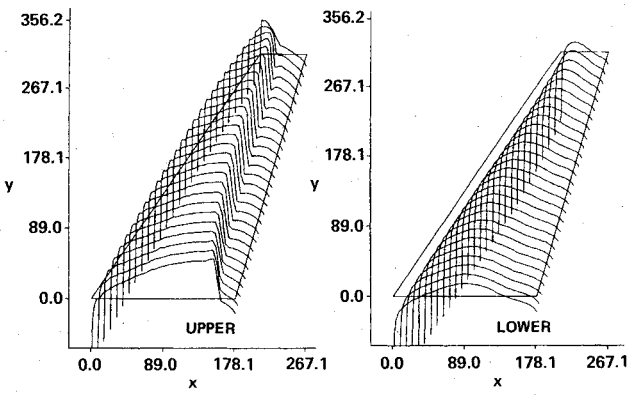

Fig. 6 Upper and lower surface pressure distribution for the base wing at $M_\infty = 0.84$ and $\alpha = 3$ deg.

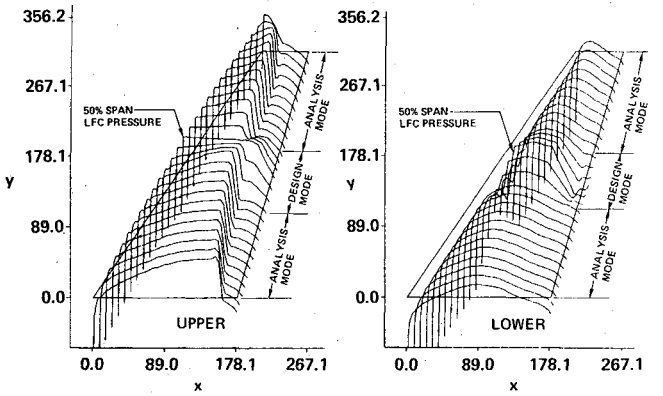

Fig. 7 Desired upper and lower surface pressure distribution to produce laminar flow control at midspan; pressure specified only in the design mode, $M_\infty = 0.84$, $\alpha = 3$ deg.

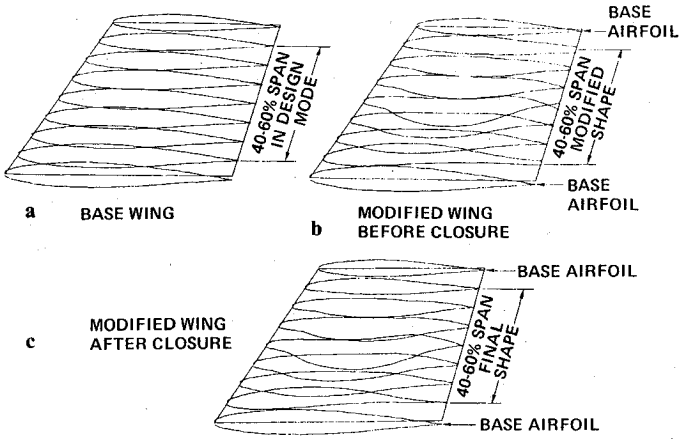

Fig. 8 Airfoil shapes for the base wing, modified wing before trailing-edge closure, and modified wing after closure.

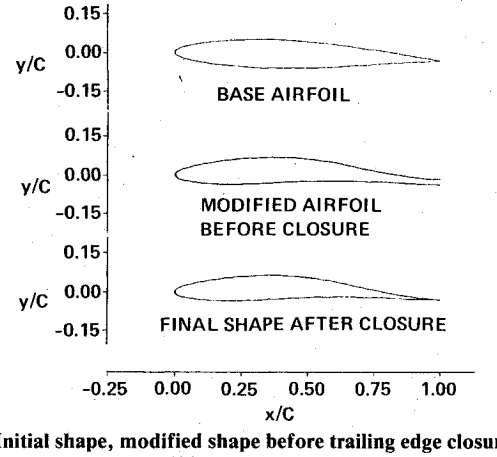

Fig. 9 Initial shape, modified shape before trailing edge closure, and final shape after closure at 40% span.

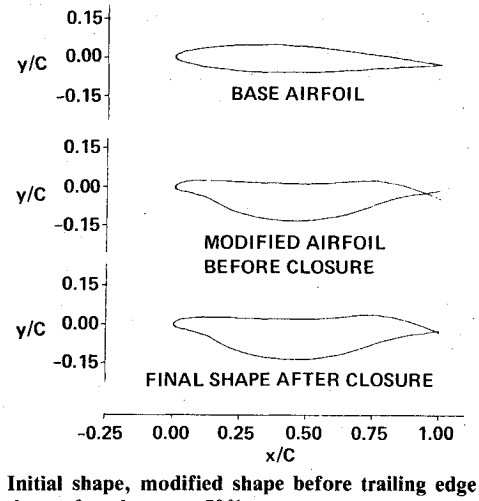

Fig. 10 Initial shape, modified shape before trailing edge closure, and final shape after closure at 50% span.

with the shape changes, the initial twist distribution is also modified to achieve the pressure distribution shown in Fig. 7.

The modified wing with closed trailing edges was then specified into the analysis code to verify the recovery of design pressure distributions. Figure 12 shows the comparison of specified pressures and recovered analysis pressures at 50.9% span station. The agreement is very good.

The entire three-dimensional analysis-design calculations as reported here required only 20 min of CPU time on the CDC 7600 computer. This reflects an enormous savings in computer cost as compared to any similar optimization program requirements.

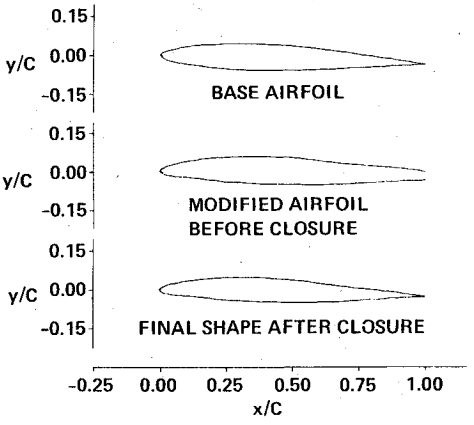

Fig. 11 Initial shape, modified shape before trailing edge closure, and final shape after closure at 60% span.

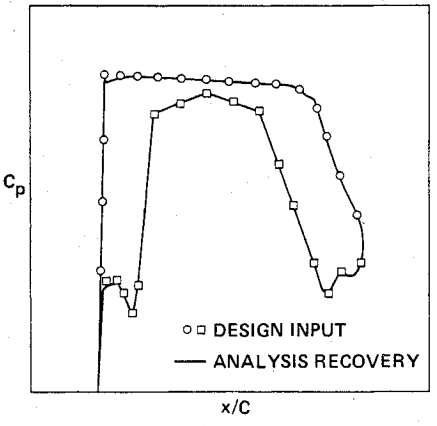

Fig. 12 Comparison of specified pressures and recovered analysis pressures for the modified wing, $M_\infty = 0.84$, $\alpha = 3$ deg, 50.9% span station.

Conclusions

An inexpensive three-dimensional inverse tool with an automated trailing-edge closure model for transonic wing design has been developed. The leading-edge velocity potentials are used as control variables to achieve trailing-edge closure. When compared to codes based on optimization methods, the present technique can save an order of magnitude in computer cost. The code in its current form can also handle wing design in the presence of a fuselage. Future extensions include wing design in the presence of a fuselage, pylon, nacelle, and winglet. The method has been validated by an analysis verification of the designed shapes. Further credence to the procedure is provided by a study of a subsonic analog.

Acknowledgments

The authors are grateful to Dr. Sukumar Chakravarthy for his sincere help in developing computer graphic capabilities and to Mr. Robert Taylor of NASA Langley for suggesting the laminar flow control design problem.

References

[1] Nieuwland, G. Y., "Transonic Potential Flow Around a Family of Quasi-Elliptical Aerofoil Sections," National Lucht-en Ruimtevaart Laboratorium, Amsterdam, NLR-TR-T. 172, 1967.

[2] Garabedian, P. R. and Korn, D. G., "Numerical Design of Transonic Airfoils," *Numerical Solution of Partial Differential Equations—II*, Academic Press, 1971.

[3] Steger, J. L. and Klineberg, J. M., "A Finite Difference Method for Transonic Airfoil Design," *AIAA Journal*, Vol. 11, May 1973, pp. 628-635.

[4] Tranen, T. L., "A Rapid Computer Aided Transonic Airfoil Design Method," AIAA Paper 74-501, June 1974.

[5]Carlson, L. A., "Transonic Airfoil Analysis and Design Using Cartesian Coordinates," *Proceedings of the AIAA 2nd Computational Fluid Dynamics Conference*, June 1975, pp. 175-183.
[6]Shankar, V., Malmuth, N. D., and Cole, J. D., "Computational Transonic Design Procedure for Three Dimensional Wings and Wing-Body Combinations," AIAA Paper 79-0344, 1979.
[7]Henne, P. A., "Inverse Transonic Wing Design Method," *Journal of Aircraft*, Vol. 18, Feb. 1981, pp. 121-127.
[8]Sobieczky, H., Yu, N. J., Fung, K. Y., and Seebass, A. R., "A New Method for Designing Shock-Free Transonic Configurations," AIAA Paper 78-1114, 1978.
[9]Fung, K. Y., Sobieczky, H., and Seebass, R., "Numerical Aspects of the Design of Shock-Free Wings and Wing-Body Combinations," AIAA Paper 79-1557, 1979.
[10]Yu, N. J., "An Efficient Transonic Shock-Free Wing Redesign Procedure Using a Fictitious Gas Method," AIAA Paper 79-0075, 1979.
[11]Fung, K. Y., Seebass, A. R., Dickson, L. J., and Pearson, C. F., "An Effective Algorithm for Shock-Free Wing Design," AIAA Paper 81-1236, 1981.
[12]Hicks, R. M. and Henne, P. A., "Wing Design by Numerical Optimization," AIAA Paper 77-1247, 1977.
[13]Allen, H. J., "General Theory of Airfoil Sections Having Arbitrary Shape or Pressure Distribution," NACA Rept. 833, 1945.
[14]Lighthill, M. J., "A New Method for Two-Dimensional Design," Memorandum Aeronautical Research Council Rept. 2112, London, 1945.
[15]Munk, M. M., "General Theory of Thin Wing Sections," NACA Rept. 191, 1924.
[16]Betz, A., "Modification of Wing-Section Shape to Assure a Predetermined Change in Pressure Distribution," NACA TM 767, 1935.
[17]Tricomi, F. G., *Integral Equations*, Interscience, New York, 1957.
[18]Milne-Thompson, L. M., *Theoretical Aerodynamics*, 3rd Ed., MacMillan and Co., London, 1958, Chap. VIII.
[19]Pfenninger, W., Reed, H. L., and Dagenhart, T. R., "Design Configurations of Advanced Supercritical Laminar Suction Airfoils," presented at the Symposium on Viscous Drag Reduction, Dallas, Tex., Nov. 1979.